Highly uniform quadrature sets for the discrete ordinates method

Thomas Camminady[1], **Martin Frank**[1], **and Jonas Kusch**[1]

[1]Karlsruhe Institute of Technology
Steinbuch Centre for Computing
Karlsruhe, Germany

thomas.camminady@kit.edu, martin.frank@kit.edu, jonas.kusch@kit.edu

ABSTRACT

We present and analyze new angular quadratures for the discrete ordinates (S_N) method that originate from the triangulation of octahedra and icosahedra. The resulting quadrature sets have several desirable properties: A highly uniform distribution of the quadrature points on the sphere, low variance of the quadrature weights, adaptive generation of quadrature points, and an underlying connectivity between quadrature points. Additionally to the demonstration of good convergence properties and their applicability within the S_N method, a companion paper will show how these quadratures can be incorporated within ray-effect mitigation techniques.

KEYWORDS: Angular quadrature, discrete ordinates, radiation transport, ray-effects.

1. INTRODUCTION

As a core ingredient of the S_N method, the choice of the quadrature set significantly affects the overall solution quality since spherical integration is approximated by using an angular quadrature. A prominent numerical artifact within the S_N method is the presence of ray-effects: Approximating the spherical integration breaks symmetries in the propagation of the solution. Consequently, even for problems that would have a radially symmetric solution, the numerical solution overemphasizes certain directions of travel while underemphasizing others. The problem of ray-effects is well known in the literature [1] and several techniques to mitigate these effects exist[2]. Additionally, several quadrature sets have been constructed, keeping the application to transport problems in mind. Some of these quadrature sets were generated with the idea to ensure positivity of quadrature weights[3], other more advanced ideas additionally emphasize high order convergence when integrating spherical harmonics and are based on finite elements[4] or discontinuous finite elements[5,6]. Quadrature sets designed for high uniformity, partially with the idea of the icosahedra rotation group have also been studied recently[7,8]. While these quadratures also consider the correct integration of spherical harmonics, we neglect this principle. This is due to a partially philosophical question: How important is it to correctly integrate spherical harmonics for highly anisotropic problems? Instead, the presented quadratures are designed under consideration of two core ideas: 1) Creating highly uniform quadrature points with low variance in the resulting quadrature weights, and 2) their interoperability within the discrete ordinates method and application to transport problems. We propose quadratures for

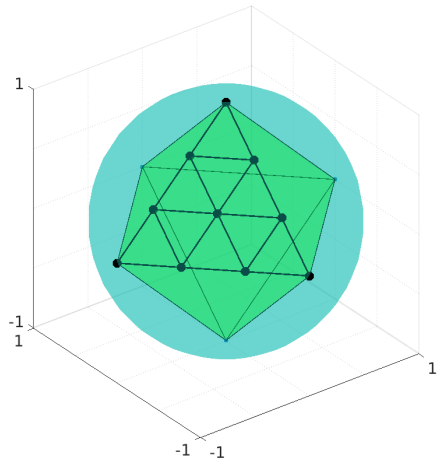

(a) Octahedron within the unit sphere, used to generate the O_N^l quadrature.

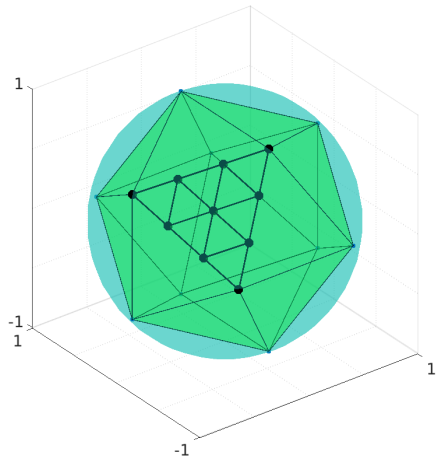

(b) Icosahedron within the unit sphere, used to generate the I_N^l quadrature

Figure 1: Generation of the quadrature sets. One face of the octahedron and icosahedron have been further refined. Vertices will be projected onto the unit sphere and taken as quadrature points.

which the quadrature points and weights can be computed at low costs and are of purely geometric nature. Due to their uniform nature, the quadratures are promising for transport problems that usually suffer from ray-effects.

Implementation of the aforementioned quadrature sets is ongoing work. A Python package will implement many state of the art quadrature sets and make them publicly available * under the name `sphericalquadpy`.

2. CONSTRUCTION OF THE QUADRATURE SETS

The considered quadrature sets can both be generated by triangulating a certain planar area. This planar area is either the face of an octahedron or of an icosahedron, respectively. The regular octahedron and icosahedron are both platonic solids. That means, they are regular, convex polyhedra with triangular faces, all having the same area. Projecting from these platonic solids onto the unit sphere yields highly uniformly distributed points on the unit sphere. This idea has been used within climate forecasting[9] where a uniform discretization of the earth's atmosphere is desirable.

The triangulation can be performed by **l**inear int**erp**olation (lerp) or **s**pherical **l**inear int**erp**olation

*The software is currently under active development and can be found here: https://github.com/camminady/sphericalquadpy

(slerp), demonstrated for the lerp version in Fig. 1a for the octahedron and in Fig. 1b for the icosahedron, respectively. Linear interpolation places points with equidistant spacing in planar geometry, whereas spherical linear interpolation places the points equidistantly on the sphere. Given two arbitrary points $p_0, p_1 \in \mathbb{R}^3$ and $t \in [0, 1]$, we perform spherical linear interpolation via

$$\text{slerp}(p_0, p_1, t) = \frac{\sin((1-t)\Omega)}{\sin(\Omega)} p_0 + \frac{\sin(t\Omega)}{\sin(\Omega)} p_1,$$

where $\cos(\Omega) = p_0 \cdot p_1$. That is, when t is being discretized equidistantly into t_i, the spherical distance between the points $\text{slerp}(p_0, p_1, t_i)$ and $\text{slerp}(p_0, p_1, t_{i+1})$ is the same for all i. Consequently, we obtain a total of four quadrature sets: O_N^l, O_N^s, I_N^l, and I_N^s. Here, O and I distinguish between the octahedron and the icosahedron version, and l and s between the lerp and slerp version, respectively. Since the difference in the construction between the octahedron and the icosahedron version is minor, we focus on the octahedron version at first. Similar to the T_N quadrature[3] the planar area is the equilateral triangle in three dimension with vertices $(1, 0, 0)$, $(0, 1, 0)$ and $(0, 0, 1)$, presented in Fig. 1a and Fig. 2a. Refining the triangulation in the planar setting and then projecting each vertex onto the sphere yields the quadrature points for one of the eight octants, shown in Fig. 2b. The quadrature weights correspond to the area associated with each quadrature point. This area is the hexagon that is defined by connecting the midpoints of the six triangles that every vertex is associated with, drawn in red in Fig. 2a and Fig. 2b. For the six poles, the associated area is a quadrilateral instead of a hexagon. By construction, all quadrature weights are therefore positive.

In contrast, the T_N method takes the triangle midpoints as the quadrature points and the associated triangle area as the quadrature weight. The slerp version of the quadrature can be constructed analogously.

For the slerp version of both quadratures, we do not perform the refinement of the triangle in planar geometry as in Fig. 2a, but instead in spherical geometry.

To obtain the icosahedron versions of the quadratures, the planar geometry is replaced by one face of an icosahedron. The procedure then works analogously.

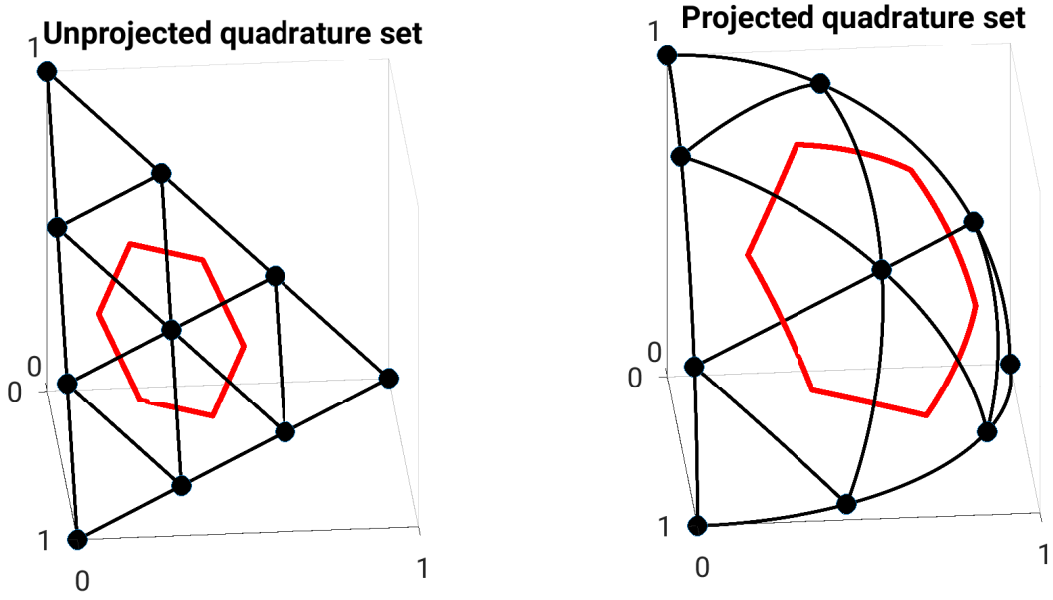

(a) The refined triangle and the associated hexagon for the centered quadrature point.

(b) The refined triangle and the associated hexagon for the centered quadrature point on the sphere.

Figure 2: Quadrature points and weights are created by refining a planar triangle and then projecting vertices onto the unit sphere.

3. STATISTICAL PROPERTIES AND NUMERICAL EXPERIMENTS

For the aforementioned quadratures, properties of the quadrature weights are presented in Fig. 6 in the appendix. As expected, the I_N versions have lower variance in the quadrature weights and smaller ratios between the maximal and minimal quadrature weights. Additionally, the slerp versions have smaller ratios and variance than the lerp versions. Combining these two effects, the I_N^l quadrature behaves similar to the O_N^s quadrature, whereas the O_N^l has the highest ratios and variance and the I_N^s quadrature the lowest ratios and variance. Numerical values can be extracted from Tab. 1 in APPENDIX A.

Together with the Lebedev, the Gauss-Legendre, and the LDFE-SA quadrature, we investigate the error decay for the integration of several different functions, both smooth and discontinuous. The functions are visualized in APPENDIX B. For every quadrature and every order we then compute the mean error by averaging the integration error over hundred random rotations of the quadrature set. We also plot the variance of the error (from mean error to worst error). While Lebedev and

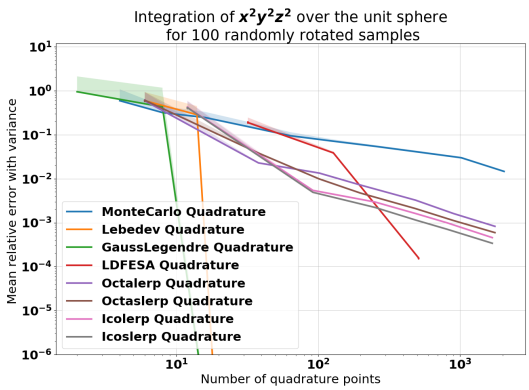

(a) Convergence for $f(x, y, z) = x^2y^2z^2$.

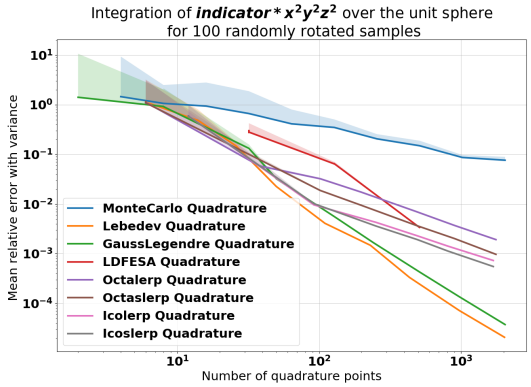

(b) Convergence for $f(x, y, z) = \text{indicator} \cdot x^2y^2z^2$. We restrict the function to one octant.

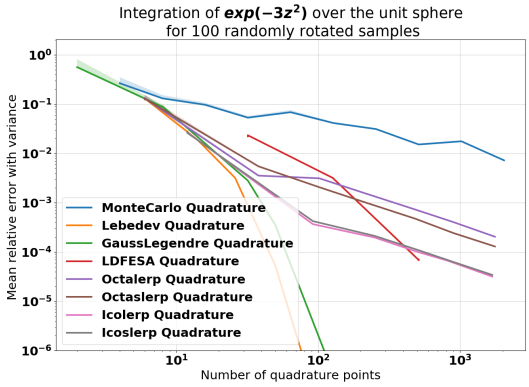

(c) Convergence for $f(x, y, z) = \exp(-3z^2)$.

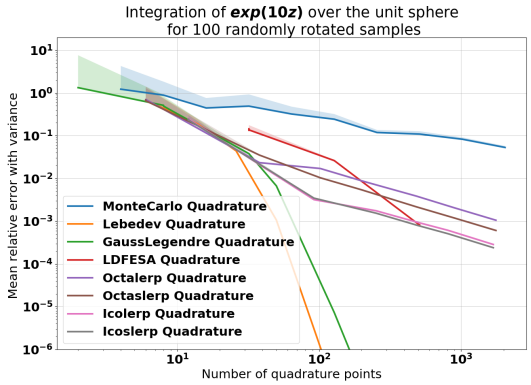

(d) Convergence for $f(x, y, z) = \exp(10z)$.

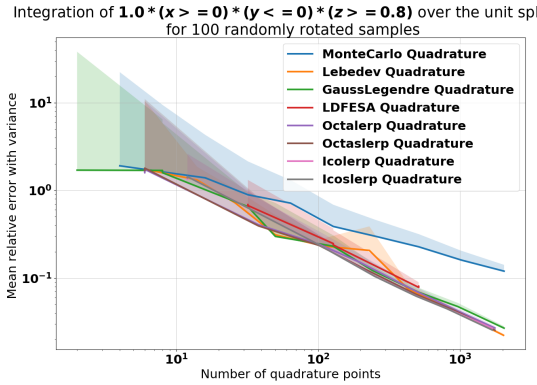

(e) Convergence for $f(x, y, z) = \text{indicator} \cdot (z > 0.8)$.

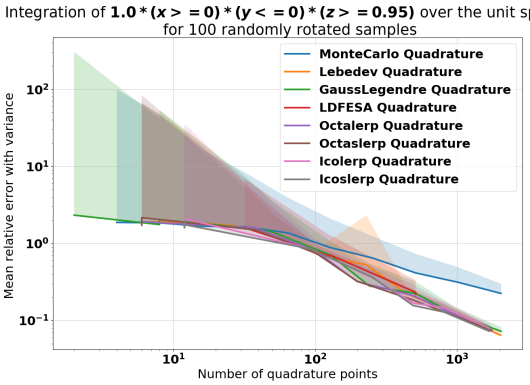

(f) Convergence for $f(x, y, z) = \text{indicator} \cdot (z > 0.95)$.

Figure 3: Convergence overview for different quadratures and functions.

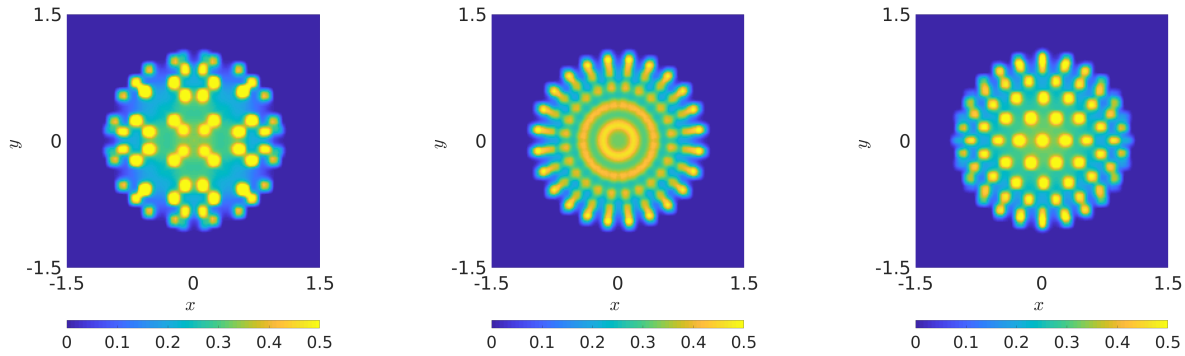

(a) LDFE-SA ($n_q = 128$) **(b) GL** ($n_q = 144$) **(c)** $\mathbf{I}_N^s$ ($n_q = 162$)

Figure 4: Solutions to the line-source problem with ray-effects.

Gauss-Legendre are able to integrate the spherical harmonics exactly after a certain order, the octahedron and icosahedron based quadratures converge with first order. For a sufficiently small power of the spherical harmonics, the LDFE-SA quadrature indicates second order convergence. However, the I_N^l quadrature beats the LDFE-SA quadrature for up to approximately 500 quadrature points in the first two cases and for all number of quadrature points in the latter cases.

Similar behavior can be observed for integrating smooth functions, i.e. $f(x, y, z) = \exp(10z)$ or $f(x, y, z) = \exp(-3z^2)$: The order of the LDFE-SA quadrature appears higher, but the advantage of the higher order starts to show up relatively late.

For a set of two highly localized, discontinuous functions the quadratures behave similar. However, we observe smaller variance for our proposed quadratures with respect to random rotations of the quadrature set (or equivalently the function living on the sphere). All functions considered in the the convergence studies are visualized in APPENDIX B.

Next, we consider solutions to the so-called line-source problem since it neatly illustrates typical problems in transport simulations. For three choices of quadratures in Fig. 5 we observe ray-effects. However, for the I_N^s quadrature, the results look more homogeneous. This can also be observed when further refining the angular quadrature. Additionally the proposed quadratures are used within ray-effect mitigation techniques, presented in a companion paper[10], where their capabilities to mitigate ray-effects are investigated.

Lastly, we briefly discuss the lattice problem[11]. Here, an isotropic source is placed in the middle of a lattice. The medium is highly heterogeneous, containing regions of high and low absorption and scattering, respectively. Due to the arrangement of the different materials, ray effect are visually observable at the outside of the computational domain when plotting the particle density. While there is no clear difference between the different quadrature sets, integrating the I_N^s into ray-effect mitigation techniques has shown to yield a drastic improvement of the overall solution quality, both for the line-source and the lattice problem[12].

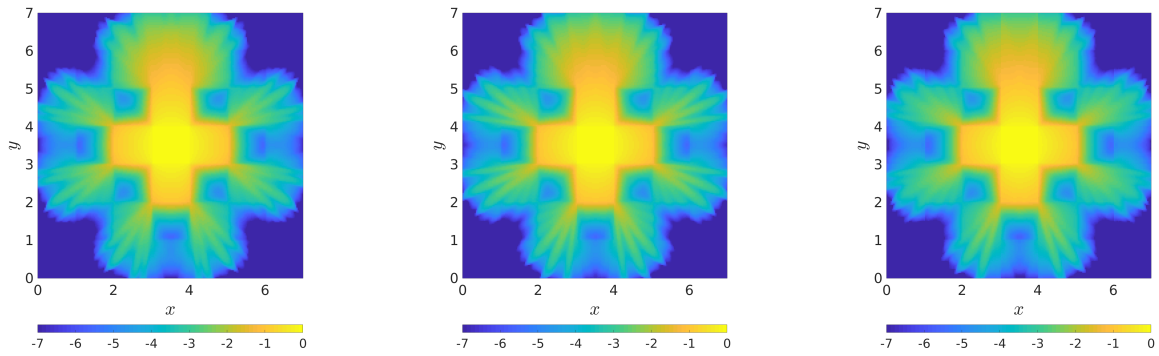

(a) LDFE-SA ($n_q = 128$) **(b) GL** ($n_q = 144$) **(c)** $\mathbf{I}_N^s$ ($n_q = 162$)

Figure 5: Solutions to the checkerboard problem with ray-effects.

4. Conclusion & Outlook

We constructed and analyzed a class of quadrature sets, designed to be 1) uniformly spread on the unit sphere and 2) usable in ray-effect mitigation techniques. The quadratures are not designed under consideration of integrating spherical harmonics but still show good convergence properties when integrating smooth and discontinuous functions.

For the line-source and lattice test case, a more quantitative analysis of the influence of the quadrature set on the solution quality will be performed with a special focus on ray-effect mitigation techniques proposed in [12] and [10]. Additionally, classical benchmark problems as proposed in [13] will be considered.

All presented quadratures will be available openly online as the software package `sphericalquadpy`, written in Python.

REFERENCES

[1] K. D. Lathrop, "Ray effects in discrete ordinates equations," *Nuclear Science and Engineering*, vol. 32, no. 3, pp. 357–369, 1968.

[2] J. E. Morel, T. A. Wareing, R. B. Lowrie, and D. K. Parsons, "Analysis of ray-effect mitigation techniques," *Nuclear Science and Engineering*, vol. 144, no. 1, pp. 1–22, 2003.

[3] C. Thurgood, A. Pollard, and H. Becker, "The TN quadrature set for the discrete ordinates method," *Journal of heat transfer*, vol. 117, no. 4, pp. 1068–1070, 1995.

[4] L. L. Briggs, W. F. M. Jr., and E. E. Lewis, "Ray-effect mitigation in discrete ordinate-like angular finite element approximations in neutron transport," *Nuclear Science and Engineering*, vol. 57, no. 3, pp. 205–217, 1975.

[5] J. J. Jarrell and M. L. Adams, "Discrete-ordinates quadrature sets based on linear discontinuous finite elements," *International Conference on Mathematics & Computational Methods Applied to Nuclear Science & Engineering*, 2011.

[6] C. Y. Lau and M. L. Adams, "Discrete ordinates quadratures based on linear and quadratic discontinuous finite elements over spherical quadrilaterals," *Nuclear Science and Engineering*, vol. 185, no. 1, pp. 36–52, 2017.

[7] D. B. Fromowitz and G. B. Zeigler, "Development and evaluation of high-fidelity product and evenly spaced angular quadratures for three-dimensional discrete ordinates calculations with large air regions," *Nuclear Science and Engineering*, vol. 182, no. 2, pp. 166–180, 2016.

[8] K. Manalo, C. D. Ahrens, and G. Sjoden, "Advanced quadratures for three-dimensional discrete ordinate transport simulations: A comparative study," *Annals of Nuclear Energy*, vol. 81, pp. 196–206, 2015.

[9] D. Rieger, M. Bangert, I. Bischoff-Gauss, J. Förstner, K. Lundgren, D. Reinert, J. Schröter, H. Vogel, G. Zängl, R. Ruhnke, *et al.*, "Icon–art 1.0–a new online-coupled model system from the global to regional scale," *Geoscientific Model Development*, vol. 8, no. 6, pp. 1659–1676, 2015.

[10] T. Camminady, M. Frank, C. Hauck, and J. Kusch, "Ray-effect mitigation for the discrete ordinates method using artificial scattering," *International Conference on Mathematics & Computational Methods Applied to Nuclear Science & Engineering*, 2019.

[11] T. A. Brunner, "Forms of approximate radiation transport," *Sandia report*, 2002.

[12] T. Camminady, M. Frank, K. Küpper, and J. Kusch, "Ray effect mitigation for the discrete ordinates method through quadrature rotation," *Journal of Computational Physics*, vol. 382, pp. 105–123, 2019.

[13] M. L. Adams and E. W. Larsen, "Fast iterative methods for discrete-ordinates particle transport calculations," *Progress in nuclear energy*, vol. 40, no. 1, pp. 3–159, 2002.

APPENDIX A. Statistics of the quadrature sets

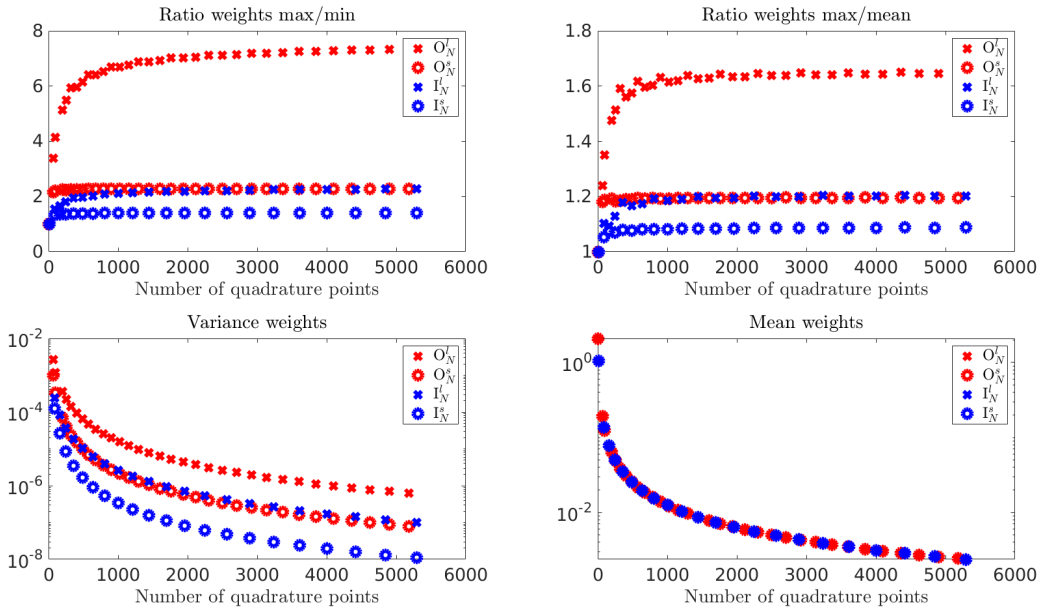

Figure 6: Statistical properties of the quadrature weights for different orders.

Table 1: Statistical properties of the quadrature weights (for $n_q \approx 5000$). Quadrature weights sum to 4π for every quadrature set.

Quadrature	ratio max/min	ratio max/mean	variance
O_N^l	7.1967	1.6467	6.224E-7
O_N^s	2.2804	1.1952	7.898E-8
I_N^l	2.2970	1.2074	9.906E-8
I_N^s	1.4119	1.0919	1.100E-8

APPENDIX B. Plots for the test cases in the convergence study

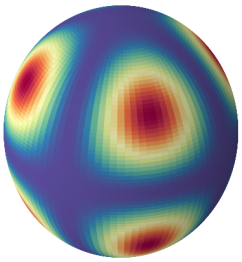

(a) Plot of $f(x, y, z) = x^2y^2z^2$.

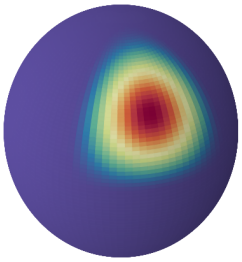

(b) Plot of $f(x, y, z) =$ indicator $\cdot\, x^2y^2z^2$. We restrict the function to one octant.

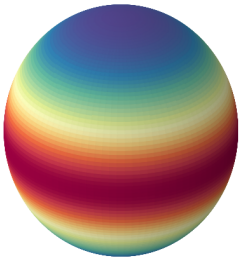

(c) Plot of $f(x, y, z) = \exp(-3z^2)$.

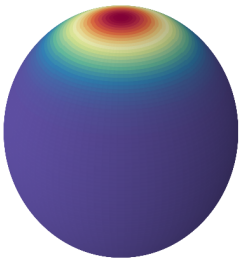

(d) Plot of $f(x, y, z) = \exp(10z)$.

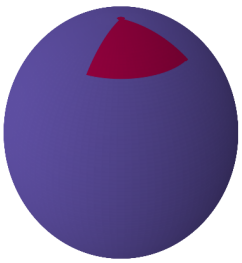

(e) Plot of $f(x, y, z) =$ indicator $\cdot\, (z > 0.8)$.

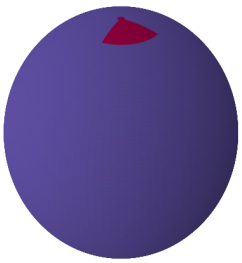

(f) Plot of $f(x, y, z) =$ indicator $\cdot\, (z > 0.95)$.